MAY 01 2006

Broadband sound reflection by plates covering side-branch cavities in a duct

Lixi Huang

J. Acoust. Soc. Am. 119, 2628–2638 (2006)
https://doi.org/10.1121/1.2186431

Broadband sound reflection by plates covering side-branch cavities in a duct

Lixi Huang[a)]
Department of Mechanical Engineering, The Hong Kong Polytechnic University, Kowloon, Hong Kong

(Received 9 December 2005; revised 3 February 2006; accepted 18 February 2006)

When a segment of a rigid duct is replaced by a plate backed by a hard-walled cavity, grazing incident sound waves induce plate bending, hence sound reflection. The mechanism is similar to the drumlike silencer with tensioned membranes [L. Huang, J. Acoust. Soc. Am. **112**, 2014–2025 (2002)]. However, the logarithmic bandwidth over which the reflection occurs is much wider than that of a drumlike silencer of the same cavity geometry, the typical difference being nearly one octave band. The difference in the silencing performance is explained in terms of the intermodal acoustic interference between the odd and even *in vacuo* vibration modes. For a given cavity volume, the widest stopband for noise in air is obtained by using long plates with two free lateral edges parallel with the duct axis. The optimal material should be stiff and light, and the critical parameter is found to be the ratio of the Young's modulus over the cube of density. Typically, this ratio is 250 times higher than those of common metallic materials like aluminum alloys, but it is within the reach of existing ultralight foam materials or composite beams with a light core. © *2006 Acoustical Society of America.* [DOI: 10.1121/1.2186431]

PACS number(s): 43.20.Tb, 43.20.Ks [KA] Pages: 2628–2638

I. INTRODUCTION

Duct noise control finds many applications such as ventilation systems in built-up environments. Medium and high-frequency noise is easily tackled by duct lining using porous materials, for which the technology is rather mature. Low-frequency noise remains a technical challenge. Active control could, in principle, deal with such problem with ease, but the actual applications of the technology have been few due to cost, reliability, and other practical concerns. The present author has been developing an alternative for the low-frequency duct noise control through the use of flexible walls (Huang, 1999) leading to a prototype device of drumlike silencer (Huang, 2002) in which a segment of tensioned membrane lines part of the duct wall, and each membrane is backed by a hard-walled cavity. Incident sound waves from upstream induce the membrane to vibrate and the vibration radiates sound in both directions of the duct. The upstream radiation forms the wave reflection while the downstream radiation combines with the incident wave and destructive acoustic interference ensues. In fact, the acoustics of such device is very similar to a successful scheme of active duct noise control using a single side-branch loudspeaker except that the secondary source in this case is the tensioned membrane, and there is absolutely no chance that the destructive acoustic interference in the downstream region could turn out to be constructive. This is so because the incident wave is the only energy source and the acoustic energy conservation guarantees that there is transmission loss of noise across such flexible segments. When compared with duct lining and splitter-type silencers, the drumlike silencer carries the extra merit of creating zero back pressure and using no porous material. The prototype device has been tested successfully for the conditions of without (Choy and Huang, 2002) and with flow (Choy and Huang, 2005).

It has been shown that the drumlike silencer achieves its best silencing performance under an optimal tensile force (Huang, 2004). When the membrane is too loose, reflection waves from different parts of the membrane simply cancel themselves out. When the membrane is too tight, it approaches the condition of a hard wall. The mechanism of the superior sound reflection capability achieved for the optimal configuration lies in the delicate acoustic interference between different parts of the tensioned membranes. If the membrane vibration is decomposed into *in vacuo* modes of velocity $\sin(j\pi x/L)$, where the membrane occupies $x \propto [0,L]$, the broadband performance is found to derive mainly from the first two modes, $j=1,2$. The first mode is very effective in reflecting low-frequency sound but is hard to excite due to the cavity air stiffness. The second mode is relatively ineffective in reflecting low-frequency sound but is rather easy to excite. The two modes are found to supplement each other in achieving a broadband silencing performance.

In this study, the tensioned membrane is replaced by a plate with its natural bending moment as the sole structural restoring force. The parametric relationship between the first two *in vacuo* modes is changed, and a corresponding change in the intermodal acoustic interference is also expected to take place. For example, the second membrane (string) mode has its eigenfrequency twice as much as that of the first mode. But, this is changed to four times when it comes to the plate. It is shown in later sections that the change in the intermodal relationship is beneficial for sound reflection provided that the parameters of the plate are optimized.

The use of a plate and, for this matter, the tensioned membrane in noise abatement may not be new, but its use as

a)Electronic mail: mmlhuang@polyu.edu.hk

 0001-4966/2006/119(5)/2628/11/$22.50

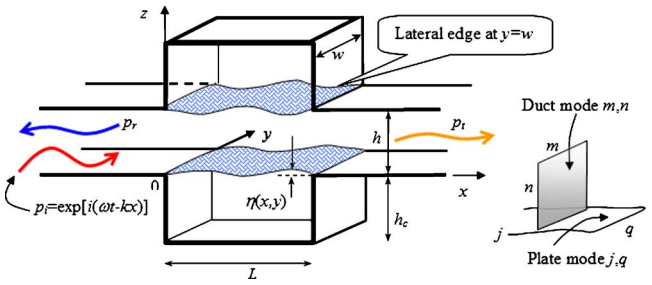

FIG. 1. (Color online) Theoretical model of sound wave reflection by two cavity-backed plates forming part of the otherwise rigid duct walls.

a side-branch wave reflector is. For example, a plate has been used as a means to adjust certain acoustic resonance. Panel absorbers are used in broadcasting studios and other architectural practices (Brown, 1964; Ford and McCormick, 1969; Horoshenkov and Sakagami, 2001), membrane absorbers are used as splitter silencers in the form of arrays of Helmholtz resonators (Frommhold *et al.*, 1994). However, in all these applications the panel, or the membrane, is a component of a resonator which works for a narrow frequency band. The structural mass is often a desirable property to achieve a low resonance frequency. Here, it is shown that the most desirable properties of a plate as a side-branch wave reflector are the high stiffness and low density.

In what follows, theoretical outlines are given in Sec. II, and the relationship between plate/cavity resonance and wave reflection is examined for the three-dimensional acoustic model and two-dimensional plate model. In Sec. III, the model is changed to two-dimensional duct and one-dimensional beam, leading to the optimal wave reflection performance. The effects of plate and cavity damping are also studied. Section IV examines the effect of plate mass and the issue of material selection.

II. THEORETICAL MODEL AND PLATE RESONANCE

A. Three-dimensional theoretical model

As shown in Fig. 1, a segment of a rigid duct of height h and width w is lined by two plates of length L and width w. Each plate is supported by a cavity of depth h_c. The four edges of the plate may have different structural boundaries. The leading and trailing edges located at $x=0,L$ are simply supported. This condition is preferred over the clamped condition for a uniform plate since it allows the plate to respond to incident waves with a higher vibration magnitude. The two lateral edges, defined as those located at $y=0,w$, can be either simply supported, as is the case in the analysis of this section, or free, which is the case for the later sections. A plane incident wave comes from the left to the right with a unit amplitude,

$$p_i = e^{i(\omega t - kx)}, \tag{1}$$

and it induces the plate to vibrate with a transverse displacement of complex amplitude $\eta(x,y)$ and velocity $V(x,y)$ with the same time dependence, $\exp(i\omega t)$, which is henceforth omitted. The plate motion radiates sound in both directions of the duct axis, $\pm x$, and it induces a fluid loading of

$$\Delta p = (\,p|_{z=0+} - \,p|_{z=0-})^{(\eta)}. \tag{2}$$

Note that Δp is defined as that induced by the plate vibration (hence the superscript η) excluding the loading by the incident wave. The plate vibration is governed by the following equation:

$$m_s \frac{\partial^2 \eta}{\partial t^2} + B\nabla^4 \eta + p_i + \Delta p = 0, \tag{3}$$

where $B=Es^3/[12(1-\nu^2)]$ is the bending stiffness, m_s, E, ν, s are, respectively, the plate mass per unit surface area, the Young's modulus, Poisson's ratio, and the plate thickness. The effect of damping is investigated in the next section where relevant formulation is given. In order to solve Eq. (3) both the plate vibration and the fluid loading on the plate are expanded into the *in vacuo* modes of the simply supported plate denoted by $\varphi_{jq}(x,y)$,

$$\varphi_{jq}(x,y) = \sin(j\pi x/L)\sin(q\pi y/w),$$

$$V(x,y) = \sum_{j=1}^{\infty}\sum_{q=1}^{\infty} V_{jq}\varphi_{jq}(x,y),$$

$$V_{jq} = \frac{4}{Lw}\int_0^w dy \int_0^L V(x,y)\varphi_{jq}dx,$$

$$\Delta p^{(\eta)} = \sum_{j,q} V_{jq} \sum_{j',q'} Z_{jqj'q'}\varphi_{j'q'}, \tag{4}$$

$$Z_{jqj'q'} = \frac{4}{Lw}\int_0^w dy \int_0^L \Delta p^{(\varphi_{jq})}\varphi_{j'q'}dx,$$

where $\Delta p^{(\varphi_{jq})}$ denotes the fluid loading induced by the modal vibration of indices (j,q) with a unit amplitude, and $Z_{jqj'q'}$ is the modal impedance defined as the fluid loading of mode (j',q') arising from the plate vibration of mode (j,q) with a unit velocity amplitude. The formulations for $Z_{jqj'q'}$ and the convergence of the solution for the truncated set of equations are documented in Huang (2002) and Huang and Choy (2005) for tensioned membranes. Since $Z_{jqj'q'}$ is the acoustic property of the duct and the cavity, it is independent of the structural mechanics. In other words, $Z_{jqj'q'}$ found for the membrane problem can also be used here. Briefly, the modal impedance problem becomes a standard radiation problem and the solution can be expanded into the duct acoustics modes (Doak, 1973) of indices m in the y direction and n in the z direction, illustrated in the right-hand part of Fig. 1. Using the standard Galerkin procedure, the following set of linear equations are obtained:

$$\mathcal{L}_{jq}V_{jq} + \sum_{j',q'} Z_{j'q'jq}V_{j'q'} + I_{jq} = 0, \quad j,q = 1,2,3,\cdots, \tag{5}$$

where $\mathcal{L}_{jq}$ is the structural mechanics operator,

$$\mathcal{L}_{jq} = m_s i\omega + \frac{B}{i\omega}\left[\left(\frac{j\pi}{L}\right)^4 + 2\left(\frac{j\pi}{L}\right)^2\left(\frac{q\pi}{w}\right)^2 + \left(\frac{q\pi}{w}\right)^4\right], \tag{6}$$

and I_{jq} is the modal excitation of the given incident wave p_i,

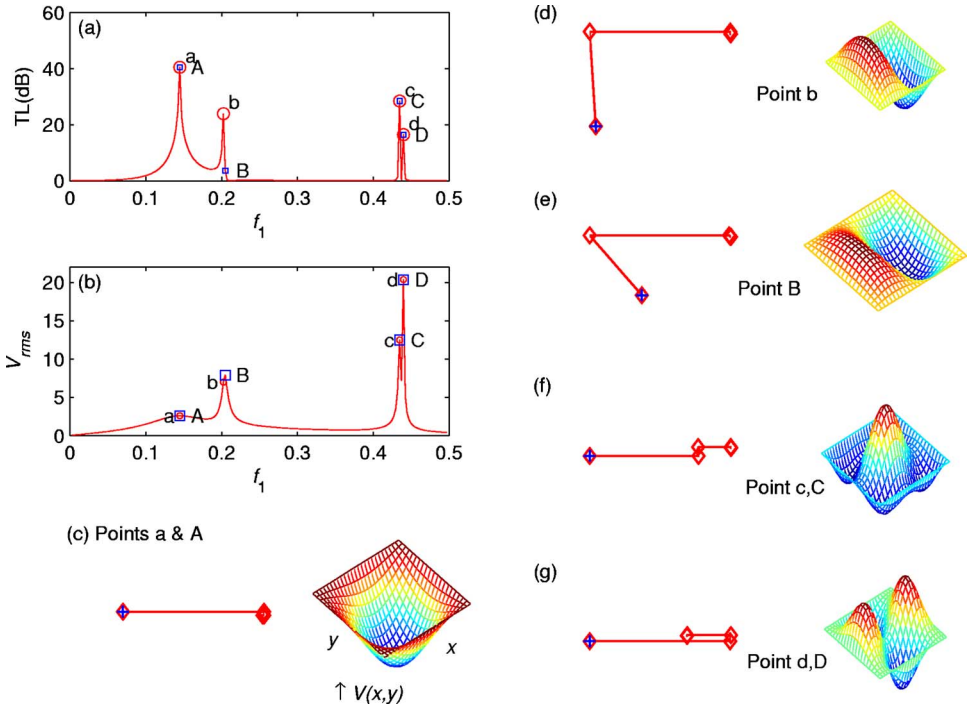

FIG. 2. (Color online) Resonance of the cavity-backed, side-branch plate with $L=h$, $h_c=h$, $B_1=0.001$. (a) System TL. (b) Plate vibration velocity (V_{rms}, relative scale). (c) Modal decomposition of the reflected sound and the instantaneous plate vibration velocity distribution for the first resonance frequency, point A, where TL also peaks. (d) Second TL peak point b. (e) Second resonance frequency point B. (f) Third and (g) fourth TL peak and resonance frequency points.

$$I_{jq} = \frac{4}{Lw}\int_0^w \left(\int_0^L p_i(x)\varphi_{jq}(x,y)dx\right)dy$$
$$= 4\frac{1-\cos(q\pi)}{q\pi} \times j\pi e^{ikL/2}\left[\frac{1-e^{i(-kL+j\pi)}}{(j\pi)^2-(kL)^2}\right]. \quad (7)$$

The set of linear equations (5) is truncated to a finite number of modes in all three dimensions: axial plate mode j, lateral plate mode q, and duct acoustics modes, m,n. Numerical tests show that the modal convergence properties for the plate problem are similar to the membrane problem, and details are not given here. In the numerical examples given below, the plate modes are truncated to 20 in both length and width directions while 50 modes are used for the duct acoustics. Once the complex modal velocity V_{jq} is obtained, the far-field sound radiation to the upstream represents the reflection wave calculated by

$$p_r = \sum_{j,q} p_{rjq} = \sum_{j=1}^{\infty} p_{rj}, \quad p_{rj} = \sum_{q=1}^{\infty} p_{rjq},$$

$$p_{rjq} = \frac{\rho_0 c_0}{2hw^2} V_{jq} \int_0^w \left(\int_0^L \varphi_{jq}(x,y)e^{-ikx}dx\right)dy, \quad (8)$$

where ρ_0, c_0 are the fluid density and speed of sound, respectively, and the contribution from each axial mode, j, is calculated by a summation over the lateral mode of index q. The radiation to the downstream combines with the incident wave to become the transmitted wave, which is written below together with the definition of the transmission loss TL,

$$p_t = p_i + \frac{\rho_0 c_0}{2hw^2}\sum_{j,q} V_{jq}\int_0^w \left(\int_0^L \varphi_{jq}(x,y)e^{+ikx}dx\right)dy, \quad (9)$$

$$\text{TL} = 20\log_{10}\frac{|p_i|}{|p_t|}.$$

When the two lateral edges at $y=0,w$ are set free, the problem is degenerated into two dimensions for the duct acoustics and one dimension for the plate (or beam). The above equations can be easily adapted by eliminating the modes in the y direction with indices q and m. The formulations for the 2D problem are similar to Huang (2002) and are not listed separately here for the sake of brevity.

In all numerical examples, parameters are normalized. Three basic normalization quantities are chosen, fluid density ρ_0, speed of sound c_0, and duct height h. Time and pressure quantities are normalized by c_0/h and $\rho_0 c_0^2$, respectively. By doing so, three most important parameters emerge,

$$f_1 = \frac{\omega h}{2\pi c_0}, \quad m_1 = \frac{m_s}{\rho_0 h}, \quad B_1 = \frac{B}{\rho_0 c_0^2 h^3}, \quad (10)$$

which are, respectively, the dimensionless frequency, the plate-to-fluid mass ratio, and the dimensionless bending stiffness. Here, a dimensionless variable is identified by a subscript of "1" added to its dimensional variable of the same symbol, while dimensional variables are used as much as possible. For the sake of comparative study, tensioned membranes are also investigated, and the relevant dimensionless tension is defined as $T_1=T/(\rho_0 c_0^2 h^2)$, where T is the dimensional tensile force applied.

B. Compact plate resonance

In order to best appreciate the fluid-plate interaction, an example of compact plate resonance is given with the following parameters:

$$m_1 = 1, \quad L = w = h_c = h, \quad B_1 = 0.001.$$

The results are shown in Fig. 2 with seven subfigures. Figure 2(a) shows the transmission loss (TL) spectrum and Fig. 2(b) the root-mean-square value of the plate vibration velocity integrated over the whole plate denoted by V_{rms}. Peaks in the TL spectrum are indicated by open circles and marked by lower-case letters, while the V_{rms} peaks are marked by open squares and upper-case letters. The two sets of peaks are shown in both subfigures. Figures 2(d)–2(g) are details of the vibration velocity distribution and the sound reflection for individual frequencies marked in Figs. 2(a) and 2(b).

As shown in Figs. 2(a) and 2(b), the first TL peak, "*a*," is over 40 dB and the same frequency position happens to be a rather flat peak of V_{rms}, denoted by "*A*." This common peak features mainly the fundamental mode vibration, $j=q=1$, shown in Fig. 2(c). In the left-hand side of Fig. 2(c), the sound reflection is decomposed into contributions from various axial modes of index j; cf. Eq. (8). The contribution of each axial mode is represented by a vector bounded by open diamonds based on the complex amplitude of the sound reflection. The vectorial summation indicates how the modal contributions interfere with each other. In this particular frequency of $f_1=0.145$ for points *a* and *A*, there is hardly any contribution from modes of $j>1$. The reason why V_{rms} is so low is as follows. At this frequency, most sounds are reflected by the plate. The plate becomes a pressure release surface, and the actual sound pressure is an antinode ($p \approx 0$) there. In other words, part of the excitation force is canceled out by the plate response. As shown in Figs 2(a) and 2(b), TL decreases when $f_1>0.145$ before it increases again, while V_{rms} decreases only slightly before it approaches its next peak. The TL peak deviates from the V_{rms} peak although they are not too far apart. At the point where the plate vibration is the highest, point "*B*," TL is actually very low. This is the best illustration of the fact that the plate resonance is not necessarily good for sound reflection. Modal decomposition of the sound reflection and the instantaneous plate vibration velocity are shown in Fig. 2(d) for point "*b*" and in Fig. 2(e) for point *B*. Figure 2(d) shows that good silencing performance is achieved when the reflections by the first two axial modes of $j=1,2$ are essentially out of phase (the vectors being perpendicular to each other). As shown in Fig. 2(e), a slight adjustment of frequency to point *B* shifts such phase relation, and the two modes interfere destructively. When the dimensionless frequency is further increased towards 0.44, two more sets of peaks are identified in Figs. 2(a) and 2(b). This time, the TL peaks also coincide with the V_{rms} peaks like the first point at $f_1=0.145$, but they can actually be separated by using a finer frequency resolution. Details of the vibration are shown in Fig. 2(f) for points "*c*" and "*C*," and Fig. 2(g) for points "*d*" and "*D*." Two observations are made here. First, the main contributions of sound reflection derive from the first and third modes, $j=1,3$. Second, the plate vibrations are very different for the two sets of peaks, although the frequencies are not too far apart.

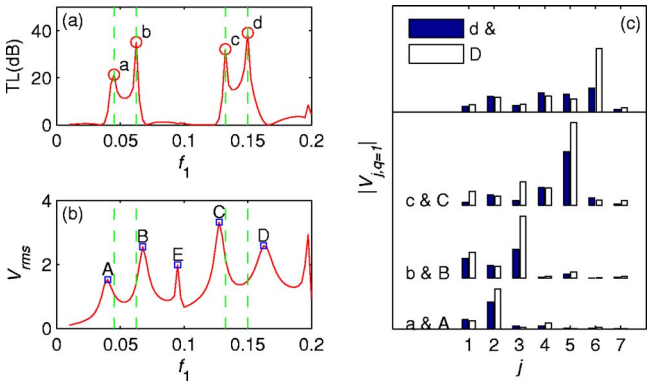

FIG. 3. (Color online) Response of a long plate with $L=5h$, $h_c=h$, $B_1=0.003$. (a) Transmission loss. (b) Root-mean-square plate vibration velocity V_{rms}. (c) Comparison of modal responses at the TL peaks (filled bars) and a nearby resonance (open bars) with frequency locations labeled in the other two subfigures.

C. Noncompact plate

The results of the short plate studies shown in Fig. 2 indicate that good silencing performance occurs near the plate resonance. This implies that, in order to obtain good low-frequency performance, the plate has to be long. The results for the following configuration:

$$m_1 = 1, \quad L = 5h, \quad w = h_c = h, \quad B_1 = 0.003,$$

are shown in Fig. 3 with frequencies zoomed in to $f_1=0$ to 0.2. For such a long plate, the first mode has very high radiation resistance and is very difficult to excite at low frequencies. Comparing the results in Figs. 3(a) and 3(b) with those of Figs. 2(a) and 2(b), there are much larger and clearer separations between the TL peaks, which are marked a,b,c,d in Fig. 3(a), and the V_{rms} peaks, which are marked by A,B,C,D in Fig. 3(b), for the long plate than for the shorter ones studied above. The resonance frequency labeled as "*E*" does not have a corresponding TL peak and is left out of the discussion. The modal amplitudes for the first peaks, *a* and *A*, are shown in the bottom row of Fig. 3(c). It is found that there is a strong second mode vibration, $j=2$, instead of the first, $j=1$, since the latter is too difficult to excite at low frequencies due to the cavity fluid stiffness. Nevertheless, the first mode still makes the dominant contribution to the sound reflection (not shown) at the first TL peak point *a*. The modal amplitudes for the second group of peak points, *b* and *B*, are shown in the second row from the bottom of Fig. 3(c). Here, the first mode response is enhanced but the third mode dominates. Point *c* and *C* feature the fifth mode, while *d* and *D* the sixth mode. It may be concluded that, for low structural bending stiffness, resonances featuring dominant axial modes occur at increasing frequencies, but not all resonance can produce a TL peak at its nearby frequencies. There is a clear frequency deviation between TL peaks and the resonance frequencies; the former generally consists of a mixture of different modes interacting constructively.

III. CAVITY AND PLATE OPTIMIZATIONS

In the previous studies for the drumlike silencer (Huang and Choy, 2005), it is found that high tension is necessary to obtain better silencing performance since a strong structure promotes low-order modes which are more effective in reflecting sound than high-order modes. However, the lateral structural constraints prohibit the overall response, and are generally unhelpful for responses at nonresonance frequencies. This is also found to be the case for plate silencer. Details are not given for such similar conclusions. In this section, a comparative study is conducted for the drumlike silencer and the plate silencer, both limited to the two-dimensional configuration in which the two lateral edges, $y=0,w$, are free to move. Since the frequency of interest is limited to that below the cut-on frequency of the duct, $f_1=0.5$, plane incident wave does not excite the lateral modes. The plate therefore behaves as a one-dimensional beam, and the duct acoustics is limited to two dimensions. The proof of such 1D structural response is given in Huang and Choy (2005) for the drumlike silencer, and is not repeated here. For simplicity, the configuration with two free lateral edges is referred to as the 2D model in the following discussions. To materialize such a 2D configuration, a small gap has to be allowed between the lateral plate edges and the duct walls. Too big a gap would cause serious leaking of sound, but a previous study for the 2D membrane configuration (Choy and Huang, 2002) showed that common design techniques used in minimizing the leakage flow between stationary and moving parts in a rotary machine would work. In the said experimental study using a duct of 5 by 5 cm cross section, a slit of 2 mm in depth was created in each lateral duct wall allowing the membrane to be inserted into the recess with an all-round clearance of no more than 0.5 mm. The experimental results demonstrated that the acoustic leakage was prevented satisfactorily. It is believed that, when the dimension of the duct cross section is increased, such gap would prevent acoustic leaking even more effectively.

In this section, the cavity shape is optimized for a given volume. The optimal shape is then fixed for the parametric study of other variables such as the plate and cavity damping. Comparative study is conducted between the plate silencer and the drumlike silencer to understand the commonality and the differences in terms of the intermodal interference.

A. Cavity shape optimization

The procedure described in Huang (2004) is followed here. For a given cavity volume, Lh_c, the aspect ratio, L/h_c, can be varied by changing the length and cavity depth simultaneously. For a given structure-to-air mass ratio, m_1, the dimensionless bending stiffness, B_1, can be varied by changing the material elasticity. The objective function is the frequency ratio, f_b/f_a, where the transmission loss, TL, is above a criterion value, $\mathrm{TL}_{\mathrm{cr}}$, over the whole frequency band $f \propto [f_a, f_b]$, or $f_1 \propto [f_{1a}, f_{1b}]$ in dimensionless form, where $f_{1a}=f_a h/c_0, f_{1b}=f_b h/c_0$. The choice of $f_b/f_a=f_{1b}/f_{1a}$ as the objective value instead of f_{1b}-f_{1a} is based on the consideration that the low-frequency noise control is a true technical challenge. The criterion value $\mathrm{TL}_{\mathrm{cr}}$ is somewhat arbitrary but a procedure described in Huang (2004) recommends that the value be chosen as the peak transmission loss for an expansion chamber whose cavity volume is three times the actual cavity volume in the silencer. For the example of volume $Lh_c=5h^2$, the criterion value thus derived is rounded up to 10 dB. This configuration and the $\mathrm{TL}_{\mathrm{cr}}$ value are adopted here. The results of the optimization are shown in Fig. 4 for the following given parameters: $m_1=1, Lh_c=5h^2$. The procedure is described as follows. With some parameters fixed as above, two variables remain: dimensionless cavity length $L_1=L/h$ and plate bending stiffness B_1. The optimization begins by fixing the value of L_1 and searching for the optimal B_1 so that f_b/f_a is the highest. This set of optimal results may be called a local optimum. The highest value of f_b/f_a for all lengths is identified as the global optimum. The local optimal parameters, f_{1a}, f_{1b}, and $B_{1\mathrm{opt}}$, are functions of the cavity length L_1, and are presented in Figs. 4(a)–4(c). Figure 4(a) shows the peak logarithmic bandwidth as a function of L_1. It is found that the global optimum is achieved right at $L_1=5$, $h_c/h=1$, since the result for $L_1=5.1$ is worse than that of $L_1=5$. Figure 4(b) shows that the dimensionless lower frequency limit, $f_{1a}=f_a h/c_0$, as a function of L_1 and the lowest f_{1a} is achieved for $L_1=5$. Figure 4(c) shows that the optimal bending stiffness, $B_{1\mathrm{opt}}$, increases with L_1 and there is no peaky appearance around $L_1=5$. The following set of optimal results is found:

$$L_{\mathrm{opt}}=5h, \quad B_{1\mathrm{opt}}=0.129, \quad f_{1a}=0.0353,$$

$$f_{1b}=4.25 f_{1a}=0.149.$$

The right-hand column of Fig. 4 shows some spectral comparisons with frequency points where $\mathrm{TL}=\mathrm{TL}_{\mathrm{cr}}$ marked by

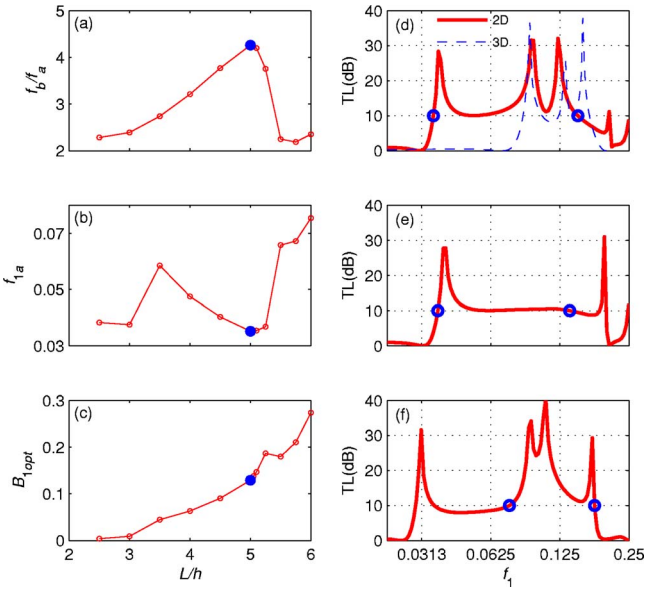

FIG. 4. (Color online) Logarithmic bandwidth optimization in terms of the B_1 and L/h while the cavity volume is fixed at $5h^2$. (a) Logarithmic bandwidth f_b/f_a. (b) Dimensionless lower bandlimit f_{1a}. (c) Dimensionless optimal bending stiffness $B_{1\mathrm{opt}}$. (d) Comparison of the optimal performance of the 2D configuration (solid line) with $L=5h$ and the optimal 3D configuration with $L=4h$ (dashed line). (e) Optimal performance for $L=5.25h$ showing a nearly flat stopband. (f) Optimal design for $L=6h$.

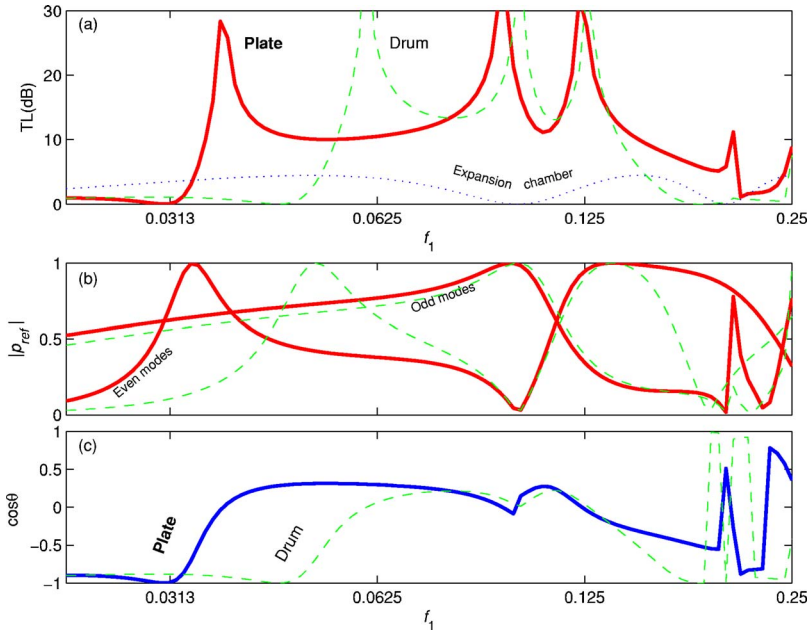

FIG. 5. (Color online) Comparison of the plate silencer (solid curves, with $B_{1\text{opt}}=0.129$) with drumlike silencer (dashed curves, with $T_{1\text{opt}}=0.475$) with the same cavity geometry of $L=5h$, $h_c=h$, and the same mass ratio of $m_1=1$. (a) TL. (b) Reflection sound decomposition into odd and even modes. (c) Odd-even interference index.

open circles for easy identification of stopbands. Figure 4(d) compares the overall optimum for $L=5h$ (solid curve) with the typical results for a three-dimensional model in which the plate is simply supported along all four edges (dashed curve) with $L=4h$, $h_c=1.25h$. The latter is not optimized under the strict criterion of $\text{TL}\geqslant\text{TL}_{\text{cr}}$ since TL=10 dB is hard to achieve for such 3D configuration described in the last section. The comparison shows that the major improvement of the 2D model from the 3D model is the low-frequency performance. The reason why the 2D configuration performs better is common with that of the drumlike silencer (Huang and Choy, 2005) and detailed analysis is not given here.

Figure 4(e) shows a very interesting 2D configuration of $L=5.25h$ for which the TL is almost flat over much of the stopband. Similar spectrum also appears for $L=5h$ when B_1 exceeds the optimal value of $B_{1\text{opt}}=0.129$, and the second and third spectral peaks merge. For the case of $L=5.25h$ shown in Fig. 4(e), the logarithmic bandwidth f_b/f_a is deemed to be lower than that of $L=5h$ due to the slight deterioration of TL near f_{1b}. Note also that there are only two spectral peaks within the band. Figure 4(f) shows that, when L_1 is further increased to 6, the bandwidth is severely narrowed due to the rather uniform drop of TL between the first two peaks in the spectrum. If the strict rule of $\text{TL}\geqslant\text{TL}_{\text{cr}}$ is somehow relaxed, it may be said that the silencer works for an ultralow frequency for a given geometry. If the dimensional frequency of interest is given, it means that the plate dimension may be reduced. For this reason, it might well be that this configuration is practically more preferable.

B. Comparison with the drumlike silencer

Coincidentally, the optimal cavity shape for the drumlike silencer for the specific volume of $Lh_c=5h^2$ is $L_{\text{opt}}=5.7h$ (Huang, 2004), not too far from $5.0h$ found for the plate silencer here. For simplicity, the performance of the drumlike silencer with $L=5h$, $h_c=h$ and the dimensionless optimal tension $T_1=0.475$ is chosen for comparative study in Fig. 5. The results for the plate silencer are shown in solid lines and those of the drumlike silencer in dashed lines. The spectral comparison is shown in Fig. 5(a) together with the performance of the expansion chamber of the same cavity geometry (dotted line). Evidently, the superiority of the plate silencer lies in the low-frequency region. Figure 5(b) compares the decomposition of the sound reflection, cf. Eq. (8) into the summation over odd *in vacuo* modes, $j=1,3,5,\ldots$ and that over the even *in vacuo* modes, $j=2,4,6,\ldots$. Focusing on the stopband below the dimensionless frequency of around 0.15, it is found that the odd-mode contribution for the two types of silencers is almost identical. For the even modes, however, the plate-type silencer outperforms the drumlike silencer with its first peak at a much lower frequency. In fact, this peak of the even-mode reflection is related to the second-mode resonance determined by the structural restoring forces (Huang, 2002), tension or bending moment, and the total mass of the coupled system. The virtual mass imposed by the cavity air is found to be much more than the structural mass for this example, and the acoustic impedance analysis for the drumlike silencer remains unchanged. The difference between the two silencers is this. For the plate silencer, a bending stiffness of $B_{1\text{opt}}=0.129$ is chosen in such a way that the second mode resonance occurs at a frequency lower than that of the drumlike silencer under $T_{1\text{opt}}=0.475$. Of course, it is also possible to choose a lower value of tension so that the second mode resonance for the drumlike silencer also occurs at a lower frequency. But, then the TL in the low-frequency regime cannot be maintained at a level above TL_{cr} due to the adverse cross-modal interference, which is shown in Fig. 5(c) as the part of the dashed curve near the label "Drum" with negative values. If the phase angle between the reflected wave from the odd modes and those of the even modes is denoted by θ, the interference index is given by $\cos\theta$, which varies from the lowest extreme of complete cancellation to complete addition. For frequency $f_1=0.03$ to 0.05, the plate silencer

works since its odd-even interference is neutral, $\cos\theta \approx 0$, while the drumlike silencer fails as its odd-even interference is rather destructive. Note that the structural responses at the three spectral peaks are rather similar to those of Huang, (2002), namely, the first peak is from the combined effect of the first and second *in vacuo* modes, the second peak is from the first mode, and the third peak is from the second mode.

C. Effects of plate and cavity damping

The effect of damping is investigated by two approaches. One is to consider various levels of structural damping on the plate, and the other is to add sound absorption materials in the cavity. For plate damping, the model adopted is written as

$$m_s(1 - i\sigma_m)\frac{\partial^2 \eta}{\partial t^2} + B\nabla^4 \eta(1 + i\sigma_s) + p_i + \Delta p = 0 \tag{11}$$

for harmonic oscillations, $\eta \propto e^{i\omega t}$, where σ_m and σ_s are, respectively, the mass and stiffness damping coefficients in the Rayleigh damping model. The mass damping coefficients acts mainly on the high-frequency oscillation while the stiffness damping on low frequencies. The exact damping mechanisms are hard to model. For the purpose of qualitative illustration, it may suffice to assume a balanced damping mechanism as

$$\sigma = \sigma_m = \sigma_s, \tag{12}$$

and focus on the overall effect of σ on the silencing performance. For the second method of adding sound absorption material into the cavity, the fluid inside the cavity is modeled as one in which the density and the speed of sound are modeled as complex quantities. Following Mechel and Vér (1992), the mass and momentum conservation laws are combined in a familiar manner to form the wave equation in the porous media,

$$\frac{1}{\rho_c c_c^2}\frac{\partial p}{\partial t} + \nabla \cdot \mathbf{v} = 0, \quad \rho_c \frac{\partial \mathbf{v}}{\partial t} + \nabla p = 0 \rightarrow \nabla^2 p - \frac{1}{c_c^2}\frac{\partial^2 p}{\partial t^2} = 0, \tag{13}$$

where $\rho_c, \mathbf{v}, c_c$ are, respectively, the complex density, particle velocity and wave speed. Note that the particle velocity is defined in such a way that $\rho_0 \mathbf{v}$ represents the true oscillating mass flow of the fluid through the porous material per unit cross section instead of $\rho_c \mathbf{v}$. Similar to sound wave propagation in lossless fluid, a velocity potential can be introduced and is related to sound pressure and velocity perturbations as follows:

$$\mathbf{v} = \nabla\phi, \quad p = -\rho_c \frac{\partial \phi}{\partial t}, \quad \left(\nabla^2 - \frac{1}{c_c^2}\frac{\partial^2}{\partial t^2}\right)\phi = 0. \tag{14}$$

The boundary condition on a solid wall with its unit normal vector $\mathbf{n}$ and the plate surface at $z=0$ are given as follows:

$$\left.\frac{\partial \phi}{\partial n}\right|_{\text{hard wall}} = 0, \qquad \left.\frac{\partial \phi}{\partial z}\right|_{\text{plate}} = \frac{\partial \eta}{\partial t}. \tag{15}$$

The sound pressure on the lower surface of the plate is obtained as $p|_{z=0-} = -\rho_c \partial\phi/\partial t$ and is used in calculating the fluid loading, $\Delta p = p|_{z=0+} - p|_{z=0-}$, used in Eq. (3). The complex wave number and impedance are given by empirical formulas (Mechel and Vér, 1992) using the data of glass fiber in the low frequency range,

$$Z_c = \rho_c c_c, \quad Z_0 = \rho_0 c_0, \quad k_0 = \omega/c_0, \quad R = -U^{-1} dp/dx,$$

$$k_c/k_0 = c_0/c_c = 0.396E^{-0.458} + i(1 + 0.135E^{-0.646}),$$

$$Z_{1c} = Z_c/Z_0 = (1 + 0.0668E^{-0.707}) - i \times 0.196E^{-0.549},$$

$$E = \rho_0 f/R \leqslant 0.025. \tag{16}$$

Note that R is the dimensional flow resistance, and a dimensionless version is defined below in the current study,

$$R_1 = \frac{Rh}{\rho_0 c_0}. \tag{17}$$

The parameters of σ and R_1 are collectively called damping factors for simplicity.

The effects of plate damping and sound absorption material filled in the cavity are investigated separately. For each type of damping mechanism and the level of damping factor chosen, the plate bending stiffness B_1 is varied to seek the widest logarithmic stopband f_b/f_a, while the geometry of $L = 5h$, $h_c = h$, and the dimensionless plate mass of $m_1 = 1$ are fixed in this optimization exercise. Again, the global optimum is identified for the highest bandwidth. The results are shown in Fig. 6. Figure 6(a) shows the optimal stopband as a function of the damping factor for the two damping mechanisms, with the global optimal point marked by a filled circle (with cavity damping) and a diamond (plate damping). For plate damping (solid line) the overall optimum is found at $\sigma_{\text{opt}} = 0.1$, $f_b/f_a = 4.54$, which is only slightly better than the bandwidth of $f_b/f_a = 4.27$ without damping. When σ exceeds around 0.12, the bandwidth suffers a sudden drop. For cavity damping (dashed line), a maximum bandwidth of $f_b/f_a = 4.84$ is achieved at $R_{1\text{opt}} = 0.07$. There is no sudden drop in bandwidth as R_1 increases further but excessive damping reduces the bandwidth. Figure 6(b) shows the optimal bending stiffness, $B_{1\text{opt}}$, as a function of the damping factors with the global optimal points shown in the same filled symbols as in Fig. 6(a). Spectral comparisons between the plate damping factors of $\sigma = 0$, σ_{opt}, 0.2 are given in Fig. 6(c). It is found that sharp peaks predicted for $\sigma = 0$ are smoothed out when there is plate damping, and excessive damping causes the TL to drop between the second and third peaks; hence, the sudden drop of f_b/f_a shown as the solid line in Fig. 6(a). The results for the cavity damping of $R_1 = 0$, $R_{1\text{opt}}$, 0.2 are shown in Fig. 6(d). It is found that the cavity damping brings a rather uniform TL across the whole frequency band, and excessive damping suppresses the responses near the lower limit of the stopband.

The contributions of the damping mechanisms towards the overall silencing effect are shown in Fig. 7 when the plate bending stiffness is fixed at its optimal value found in Fig. 6. For a plate with damping, the optimal value of $B_{1\text{opt}} = 0.132$ is given and the results are shown in Fig. 7(a). With the optimal damping factor of $\sigma_{\text{opt}} = 0.1$ (thick solid line), the average contribution of sound absorption by the damped

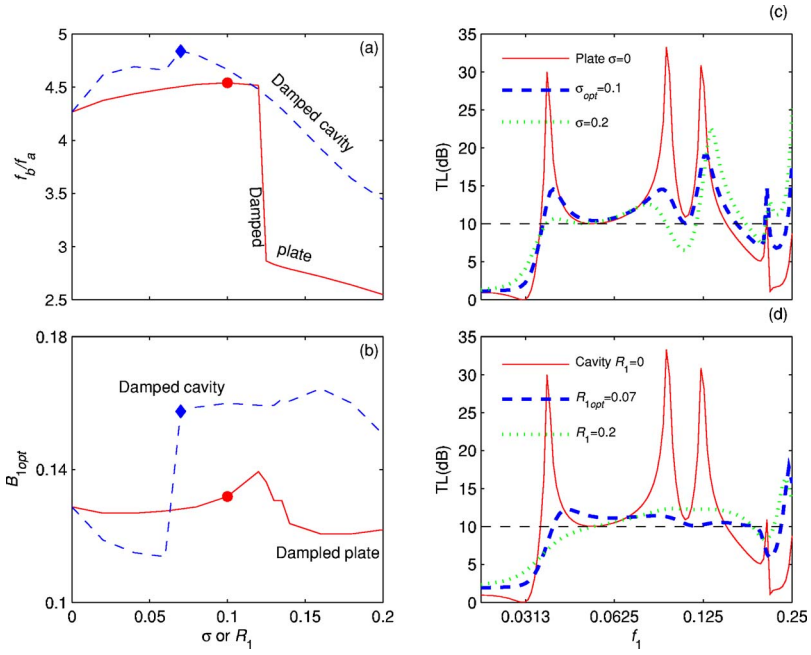

FIG. 6. (Color online) Effect of plate damping and porous material filled cavity for $L=5h$, $h_c=h$. (a) Logarithmic bandwidth. (b) Optimal bending stiffness. (c) Spectral comparison for plates with various damping factors. (d) Spectral comparison for cavity filled with sound absorption materials of various flow resistance.

plate is around 9% in the stopband marked by the two thin vertical lines. When the damping factor is increased to 0.2, the sound absorption is indeed increased to an average of 16%, but the overall TL is reduced, as shown in Fig. 6(c), due to the reduced sound reflection. For a plate without damping but the cavity filled with sound absorption material, the optimal bending stiffness is $B_{1\text{opt}}=0.158$ and the results are shown in Fig. 7(b). The contribution of sound absorption in this case is much more prominent than that of plate damping. Within the stopband marked by the two thin vertical lines, the average contribution by the cavity damping is 46% when $R_{1\text{opt}}=0.07$ is used, and is 63% when a higher value of $R_1=0.2$ is used. Again, excessive use of sound absorption mechanism stifles the plate response and reduces the overall transmission loss.

IV. EFFECT OF PLATE MASS AND CHOICE OF MATERIAL

A. Effect of plate mass

The effect of plate mass is investigated by varying the plate-to-air mass ratio m_1 while the geometry is fixed as $L=5h$, $h_c=h$. For each mass ratio given, bending stiffness is varied to find the optimal bandwidth f_b/f_a. The results are shown in Fig. 8. Figure 8(a) shows the optimal bandwidth as a function of m_1. All calculated points are marked by crosses. The overall optimum is shown by a filled triangle, while the result for $m_1=1$ is shown by a filled square. The horizontal scale is logarithmic except the special point of $m_1=0$, which is shown as an open circle. For the range of $m_1=0.05$ to 0.5, the bandwidth hovers around $f_b/f_a\approx 6.0$ with the overall optimum located at $m_1=0.25$. Figure 8(b) gives $B_{1\text{opt}}$ as a function of m_1 which shows a monotonous trend of increase. Figures 8(c) and 8(d) compare the optimal spectra for different values of m_1. Figure 8(c) explains why the bandwidth of $m_1=0$ suffers from a sudden drop of f_b/f_a from $m_1=0.05$ to 0.01 in Fig. 8(a). The reason is found as the mild decrease of TL between the first and second spectral peaks. For practical purposes, such drop can be ignored and a general conclusion can be drawn that a lighter plate provides wider stopband. Figure 8(c) also shows that, when the plate mass is increased, the stopband shrinks from both low and moderately high frequencies. Figure 8(d) shows the overall optimum (thick solid line) of $m_1=0.25$, and a rather heavy plate of $m_1=10$ (dashed line). The latter has nearly one octave stopband ranging from $f_1=0.029$ to 0.055. The bandwidth may be low, but the location in the very low frequency region could prove to be a practical advantage for the noise control at very low frequencies. In addition, a higher mass ratio also makes it easier for such a plate to be realized with a low-cost material and structure.

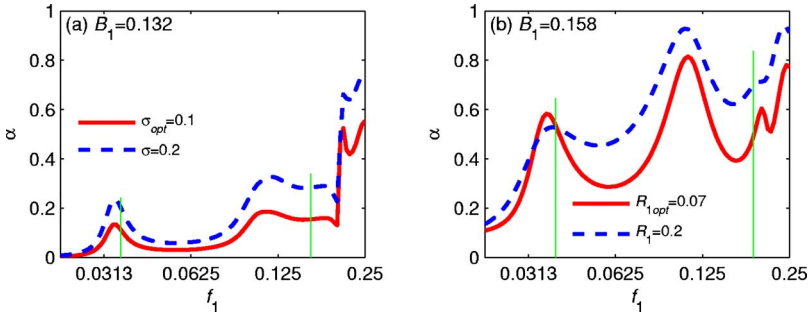

FIG. 7. (Color online) Absorption coefficient of sound energy, α. (a) Damped plate with $B_1=0.132$; (b) damped cavity with $B_1=0.158$.

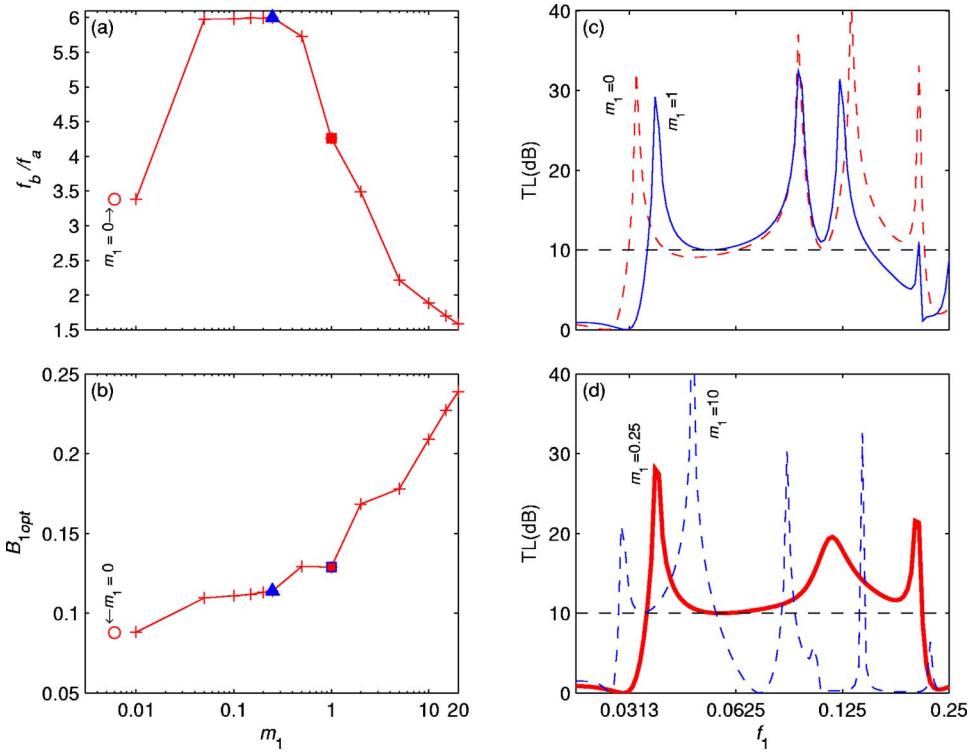

FIG. 8. (Color online) Effect of mass on (a) logarithmic bandwidth f_b/f_a, and (b) dimensionless optimal bending stiffness $B_{1\text{opt}}$, with spectral comparisons for (c) light, and (d) heavy plates. The cavity geometry is $L=5h$, $h_c=h$.

B. Choice of plate material and structure

As is shown below, it is generally difficult to satisfy the condition of a high bending stiffness with a low mass ratio. Stiffness-enhancing structures may have to be used. Denote the overall thickness of the plate as s and the volume density of the plate as ρ_s, which may be much lower than the density of the core material. The dimensionless bending stiffness, mass ratio, and the dimensional moment of inertia I are expressed below,

$$B_1 = \frac{EI}{\rho_0 c_0^2 w h^3}, \quad m_1 = \frac{\rho_s s}{\rho_0 h}, \quad I = \int_A y^2 dA = Cwh^3, \quad (18)$$

where the constant C is 1/12 for a homogeneous plate of rectangular cross section and the ratio of the actual value of C to the normal value of 1/12 can be called stiffness efficiency for a sandwich beam construction. Substituting the thickness s by $m_1 h\rho_0/\rho_s$, the dimensionless bending stiffness can be rewritten as follows:

$$B_1 = Cm_1^3 \frac{E}{\rho_0 c_0^2}\left(\frac{\rho_0}{\rho_s}\right)^3. \quad (19)$$

For a given material and sandwich beam construction, the most influential parameter is the dimensionless mass ratio m_1. When the mass ratio is increased by increasing the plate thickness, the required optimal bending stiffness also increases, cf. Fig. 8(b), and the bandwidth reduces, cf. Fig. 8(a). For $m_1=0.5,1,5$, the required values of the optimal bending stiffness are $B_1=0.114$, 0.1289, and 0.1780. The increase of $B_{1\text{opt}}$ with respect to m_1 is mild, roughly proportional to $m_1^{0.15}$ in this region of mass ratio. In other words, the requirement for $B_{1\text{opt}}$ is much easier to satisfy if the allowed mass ratio is increased with the price of having a much smaller stopband. For $m_1=5$, the logarithmic bandwidth is $f_b/f_a=2.2$. If this performance is accepted as the lower limit of a design, the mass ratio as high as 5 is considered to be relevant, and is included in the following analysis alongside the moderate mass ratio of unity.

Equation (19) also shows that, for a given set of m_1, B_1 to be satisfied, the most crucial material property is E/ρ_s^3, which is typical in the selection of weight-saving materials in aerospace applications. According to Chart 1 given in Ashby (1999), and Ashby and Johnson (2002), the best material for this purpose would be balsa, a type of wood, polyvinychloride (PVC), a type of polymer, or carbon fiber-reinforced polymer. Two materials are examined here using the normal rectangular cross section for the plate, for which $C=1/12$. The first material is the aluminum alloy with $\rho_s=2700$ kg/m^3, and $E=75$ GPa. Taking the air properties as $\rho_0=1.225$ kg/m^3, $c_0=340$ m/s, the dimensionless bending stiffness calculated by Eq. (19) is $B_1=4.12\times10^{-6}$, 5.15×10^{-4} for the mass ratios of 1 and 5, respectively, far below the required values of 0.1289 and 0.1780. It is concluded that a simple aluminum plate is about 250 times too elastic for a plate silencer even with a mass ratio of 5. The second material chosen is the PVC foam with $\rho_s=40$ kg/m^3, and $E=200$ MPa, a set of moderate values taken from Chart 1 of Ashby and Johnson (2002). The relative bending stiffness is found as $B_1=0.0034, 0.4226$ for the mass ratios of 1 and 5, respectively. In fact, this material would satisfy the optimal bending stiffness condition shown in Fig. 8(b) when the mass ratio is around 3.5.

A composite beam with a light core material like PVC foam bonded together with aluminum facings can be employed to achieve the effect of having an overall stiffness determined mainly by the elastic modulus of aluminum while the total mass is reduced drastically by the light core. Sandwich beams with honeycomb, I-beam, or corrugated

cores may also be considered to achieve the same purpose. Among the above structures, the I-beam made of a homogeneous material is perhaps most suitable for the purpose of illustrating how such structures can help satisfy the parametric requirement predicted by the current study. An I-beam cross section is mainly characterized by its depth, here denoted as s, and its flange width, w. Take the standard I-beam designated as S380×74 as an example. It has a depth of $s=381$ mm and width $w=143$ mm, the latter being roughly twice the second designation number, cf. Gere (2004). The discussion here is limited to the shape instead of the actual dimension of w and s. As listed in the tables of Gere (2004), the moment of inertia is $I=201\times10^6$ mm^4 and the cross section is 9500 mm^2. To achieve the same moment of inertia I, a plate of rectangular cross section must have a different depth s calculated by $I=\frac{1}{12}ws^3$, $s=\sqrt[3]{12I/w}\approx256$ mm. The cross section of such rectangular plate is $256\times143=36\,608$ mm^2, which is $36\,608/9500=3.85$ times that of the I-beam of the same moment of inertia. In other words, the weight-saving efficiency for such a typical I-beam is 3.85. Since the PVC foam described above can satisfy the parametric requirement of the plate silencer when the structure-to-air mass ratio is about 3.5, the weight-saving efficiency of 3.85 means that an I-beam made purely by PVC foam can satisfy the parametric requirement with a mass ratio of less than 1.0. The use of a thin rigid facing material would further enhance the structural rigidity for any given thickness s. As a result, the requirement of very light core material can be further relaxed. It is expected that a more common material like balsa may be adopted in a sandwich structure.

When using such smart structures, however, care must be taken to check whether the composite structure vibrates as one piece as assumed by the theoretical model, and whether the structural damping coefficient is low enough to allow vigorous plate response to achieve a high degree of sound reflection. More practical work needs to be done in this aspect, but it is argued that the optimal parameters predicted in this study are entirely within the reach of existing known light materials possibly with the help of composite beam construction.

V. CONCLUSIONS

This theoretical study reveals that, in a duct, a plate covering a side-branch rigid cavity can function effectively as a low-frequency wave reflector over a very broad frequency band, about one octave band broader than a drumlike silencer of the same cavity geometry. Effects of various boundary conditions and parameters are investigated. The following specific conclusions are made:

(1) When all edges of the plate are restrained to the duct walls, the response of the plate under grazing incident waves shows various axial and lateral vibration modes which consist of a combination of *in vacuo* modes in both directions depending on the excitation frequency and plate stiffness. Although the transmission loss depends very much on the magnitudes of the induced plate vibration, the spectral peaks in the plate vibration velocity, e.g., resonances, do not necessarily correspond to the peaks in the spectrum of the transmission loss. The latter depends more crucially on the acoustic interference between the wave reflections from various vibration modes. When the plate is simply supported at the leading and trailing edges and is free at the two lateral edges, the performance of the plate silencer is much better than when all edges are fixed.

(2) The first *in vacuo* plate vibration mode is effective in reflecting sound but is difficult to excite due to cavity stiffness. The second *in vacuo* mode is easy to excite but its capability to cause sound reflection is significant only when there is significant phase difference of sound over the length of the plate. The acoustic interference between the odd and even *in vacuo* modes is crucial to achieving a broad stopband. The mechanics of the plate bending differs from that of a tensioned membrane, leading to a different pattern of acoustic interference in favor of the plate silencer towards the ultralow frequencies like $f_1=0.03$.

(3) The effect of plate mass is generally counterproductive, but zero mass is not quite the optimal configuration, which differs somewhat from the drumlike silencer. The effect of the plate damping is marginally beneficial for the bandwidth, so is the use of sound absorption material in the covered cavity. However, the contribution of sound absorption in the overall noise abatement is higher in the latter case. This result can be easily understood since a highly damped plate generally responds less to the incoming sound. In other words, the effect of damping on the reduction of sound reflection is more serious when the damping is embedded in the plate motion than if it is distributed in the cavity.

(4) The optimal parameters predicted for sound reflection in air require a plate material which is very light and yet extremely stiff. When aluminum is considered, it is found that the Young's modulus E is at least 250 times too low. The critical parameter is E/ρ_s^3, for which nonmetallic materials like PVC foam can easily satisfy the requirement. In addition, composite beam structure can be used to reduce the crucial structural mass while achieving a fairly high structural stiffness.

ACKNOWLEDGMENT

The research reported here is supported by grants from the Research Grants Council of the Hong Kong SAR (PolyU 5169/02E, 5298/03E).

Ashby, M. F. (**1999**). *Material Selection in Mechanical Design*, 2nd ed. (Butterworth Heinemann, Oxford).

Ashby, M. F., and Johnson, K. (**2002**). *Material and Design: the Art and Science of Material Selection in Product Design* (Butterworth Heinemann, Oxford).

Brown, S. (**1964**). "Acoustic design of broadcasting studios," J. Sound Vib. **1**, 239–257.

Choy, Y. S., and Huang, L. (**2002**). "Experimental studies of a drumlike silencer," J. Acoust. Soc. Am. **112**, 2026–2035.

Choy, Y. S., and Huang, L. (**2005**). "Effect of flow on the drumlike silencer," J. Acoust. Soc. Am. **118**(5), 3077–3085.

Doak, P. E. (**1973**). "Excitation, transmission, and radiation of sound from source distributions in hard-walled ducts of finite length. I. The effects of duct cross-section geometry and source distribution space-time pattern," J. Sound Vib. **31**, 1–72.

Ford, R. D., and McCormick, M. A. (**1969**). "Panel sound absorbers," J. Sound Vib. **10**, 411–423.
Frommhold, W., Fuchs, H. V., and Sheng, S. (**1994**). "Acoustic performance of membrane absorbers," J. Sound Vib. **170**, 621–636.
Gere, J. M. (**2004**). *Mechanics of Materials*, 6th ed. (Brooks/Cole, London).
Horoshenkov, K. V., and Sakagami, K. (**2001**). "A method to calculate the acoustic response of a thin, baffled, simply supported poroelastic plate," J. Acoust. Soc. Am. **110**, 904–917.
Huang, L. (**1999**). "A theory of passive duct noise control by flexible panels," J. Acoust. Soc. Am. **106**(4), 1801–1809.
Huang, L. (**2002**). "Modal analysis of a drumlike silencer," J. Acoust. Soc. Am. **112**, 2014–2025.
Huang, L. (**2004**). "Parametric studies of a drumlike silencer," J. Sound Vib. **269**, 467–488.
Huang, L., and Choy, Y. S. (**2005**). "Vibroacoustics of three-dimensional drum silencer," J. Acoust. Soc. Am. **118**(4), 2313–2320.
Mechel, F. P., and Vér, I. L. (**1992**) "Sound-absorbing material and sound absorbers," *Noise and Vibration Control Engineering: Principles and Applications*, edited by L. L. Beranek and I. L. Vér (Wiley, New York), Chap. 8.